

The Nature and Origin of $z_a \approx z_e$ Absorption Lines in the Redshift 0.20 Quasar, PKS 2135–147

FRED HAMANN¹, E. A. BEAVER, ROSS D. COHEN,
VESA JUNKKARINEN, R. W. LYONS & E. M. BURBIDGE

*The Center for Astrophysics and Space Sciences, University of California – San Diego,
La Jolla, CA 92093-0424*

ABSTRACT

We use new UV and optical spectra and an archival *HST*-WFPC2 image to study the $z_a \approx z_e$ absorber in the $z_e \approx 0.20$ QSO PKS 2135–147. The UV spectra, obtained with *HST*-FOS, show strong $z_a \approx z_e$ absorption lines of C IV, N V, O VI, Ly α and Ly β . The $z_a \approx z_e$ line profiles are resolved, with deconvolved FWHM of 270 to 450 km s⁻¹. The Lyman decrement and the O VI and N V doublet ratios indicate that there are also narrower, optically thick line components, and there is evidence in the C IV and Ly α profiles for two blended components. Lower limits on the total column densities are of order 10¹⁵ cm⁻² for all ions. The $\sim 2:1$ ratio of the C IV doublets suggests that the total C IV column density is near the lower limit. If the absorber is photoionized by the QSO and the derived relative columns in C IV and H I are roughly correct, then the metallicity must be at least solar.

The location of the $z_a \approx z_e$ absorber remains uncertain. The line redshifts indicate that the clouds have little radial motion (less than ± 200 km s⁻¹) with respect to the QSO. This small velocity shift could mean that the absorber is outside of the deep gravitational potential of the QSO and the host-galaxy nucleus. Two $\sim L_*$ galaxies in a small cluster centered on PKS 2135–147 lie within $36h^{-1}$ kpc projected distance and have redshifts consistent with causing or contributing to the $z_a \approx z_e$ lines. The extensive halo of the QSO's host galaxy could also contribute. Calculations show that the QSO is bright enough to photoionize gas up to O VI in the low-density halos of the host and nearby cluster galaxies. Nonetheless, there is indirect evidence for absorption much nearer the QSO, namely (1) the derived high (albeit uncertain) metallicity, (2) the relatively strong N V absorption lines, which might be caused by a higher nitrogen abundance in the metal-rich gas, and (3) strong, lobe-dominated steep-spectrum radio emission, which is known to correlate with a much higher incidence of (probably intrinsic) $z_a \approx z_e$ lines.

We propose that the C IV/N V/O VI line ratios can be used as a general diagnostic of intrinsic versus intervening absorption, as long as the line saturation effects are understood.

Subject headings: quasars: absorption lines — quasars: individual (PKS 2135–147) — ultraviolet: galaxies

¹fhamann@ucsd.edu

1. Introduction

The working definition of associated ($z_a \approx z_e$) absorption lines in QSO spectra is that they appear within several thousand km s^{-1} of the emission-line redshift and have profile widths of less than a few hundred km s^{-1} (Weymann *et al.* 1979, Foltz *et al.* 1986, Anderson *et al.* 1987, Foltz *et al.* 1988). These systems are known statistically to comprise an independent class of absorber (Foltz *et al.* 1986), but their nature is generally uncertain. The relatively narrow line profiles distinguish $z_a \approx z_e$ features from the well-known broad absorption lines (BALs) that appear in 10% to 15% of QSO spectra (Weymann *et al.* 1991). However, there are also transitional absorbers, with intermediate line widths and sometimes high BAL-like velocities, that reveal a wide range of absorption properties between the extremes represented by BALs and the classic $z_a \approx z_e$ systems (Barthel *et al.* 1997, and Hamann *et al.* 1997a, 1997b and 1997c). BALs and transitional “mini-BALs” clearly form in QSO outflows with velocities that sometimes exceed $0.1c$ (see also Turnshek 1988). The classic $z_a \approx z_e$ systems can have a variety of origins (Weymann *et al.* 1979). A few $z_a \approx z_e$ absorbers are now known to be “intrinsic” to the QSO (forming near the QSO engine) based on (1) line strength variabilities, (2) multiplet ratios that imply partial line-of-sight coverage of the background emission source(s), or less conclusively, (3) smooth and relatively broad line profiles when observed at spectral resolutions close to the thermal speeds (Hamann *et al.* 1997a, Hamann *et al.* 1997b, Barthel *et al.* 1997, Aldcroft *et al.* 1997). The known intrinsic $z_a \approx z_e$ systems also originate in QSO ejecta; they are blueshifted with respect to the emission lines and probably form within at least a few tens of pc of the central engine. Recent studies showing typically high metallicities in $z_a \approx z_e$ systems (Møller *et al.* 1994, Petitjean *et al.* 1994, Hamann 1997), consistent with the metallicities derived from other clearly intrinsic features like the BALs and the broad emission lines (Hamann & Ferland 1993, Ferland *et al.* 1996, Turnshek *et al.* 1996, Hamann 1997), suggest that *most* $z_a \approx z_e$ lines have an intrinsic origin. Similarly, the higher incidence of $z_a \approx z_e$ lines in radio-loud vs. radio-quiet QSOs, and the further correlation between $z_a \approx z_e$ occurrence and radio properties such as the spectral index and the core/lobe flux ratio, also argue for a frequent intrinsic origin (Foltz *et al.* 1988, Wills *et al.* 1995).

However, particular $z_a \approx z_e$ systems could still form far from the QSOs, for example in the QSO’s own host galaxy (e.g. in the galactic halo) or in other galaxies along our line-of-sight. The finding that radio-loud quasars have more nearby galaxies than radio-quiet QSOs (Smith & Heckman 1990), in addition to being more likely to have $z_a \approx z_e$ lines (Foltz *et al.* 1988), has fueled speculation that neighboring galaxies (e.g. in the same galaxy cluster) often cause $z_a \approx z_e$ absorption. Some studies have placed upper limits on the absorber gas densities that require distances not less than a few tens to a few hundred kpc from the QSO (Williams *et al.* 1975, Morris *et al.* 1986). We will call all of these non-intrinsic systems “intervening” because they are probably similar (or identical) to the well-studied metal-line systems that appear far from the QSO redshifts (i.e. at $z_a \ll z_e$; Bergeron 1988).

PKS 2135–147 (PHL 1657) is a radio-loud QSO with an emission-line redshift of $z_e \approx 0.20$ and strong $z_a \approx z_e$ absorption lines that were first measured in $\text{Ly}\alpha$, C IV and N V with the *International Ultraviolet Explorer* (*IUE*; Bergeron & Kunth 1983). The absorber is the lowest redshift $z_a \approx z_e$ system known among QSOs and, as such, could help us understand the possible relationship between the $z_a \approx z_e$ systems in high-redshift QSOs and similar features in low-redshift Seyfert 1 galaxies. PKS 2135–147 is also interesting because the QSO lies near the center of a small cluster of galaxies (Stockton 1978, Stockton 1982, Bergeron & Boisse 1986, Fisher *et al.* 1996) and is surrounded by diffuse emission due to its own host galaxy (Hickson & Hutchings 1987, Véron-Cetty & Woltjer 1990, Hutchings & Neff 1992, Dunlop *et al.* 1993). Redshifts published for the QSO (Bergeron & Boisse 1986), its host galaxy and several nearby galaxies (Stockton 1978, Stockton 1982) are all similar to the $z_a \approx z_e$ redshift measured by *IUE*, leaving any (or all) of these objects as candidates for the $z_a \approx z_e$ absorber.

Figure 1 shows an image of the PKS 2135–147 field obtained by J. Bahcall and collaborators (Bahcall *et al.* 1997) on 1994 August 14 using the Wide Field and Planetary Camera 2 (WFPC2) on board the *Hubble Space Telescope* (*HST*). The diffuse emission near the QSO is not well displayed in Figure 1 but extends over $>10''$ diameter and thus encompasses the compact companion (labeled A in the figure) $1.9''$ SE of the QSO and the nearby galaxy (labeled 1) $5.5''$ to the SE. The linear scale at the redshift of the QSO is $\sim 2.2h^{-1}$ kpc arcsec $^{-1}$ for $h \equiv$

$H_o/(100 \text{ km s}^{-1} \text{ Mpc}^{-1})$. The luminosity surrounding PKS 2135–147 has a galaxy-like spectrum with stellar absorption features and [O III] emission lines (Stockton 1982, Hickson & Hutchings 1987, Stockton & MacKenty 1987). The compact object A lies well within the host galaxy defined by this diffuse luminosity and could be a secondary nucleus (Stockton 1982). It has strong line emission and an apparently non-thermal flux distribution, suggesting low-level QSO-like (or Seyfert nucleus-like) activity (Stockton 1982).

Table 1 lists coordinates for all the bright sources in Figure 1 as determined by us from the flux centroids. The maximum (3σ) errors in the relative positions should be $<0.1''$ unless noted otherwise in the table. The errors in the absolute positions could be as large as $1.5''$ (according to the *WFPC2* Instrument Handbook, Version 3.0); however, there is good agreement between the quasar coordinates in Table 1 and the radio core position (see table legend). The redshift of PKS 2135–147 shown in Figure 1 (also Table 1) was measured by us from the narrow emission lines in the QSO spectrum (see §2.2.1 below). The remaining redshifts are from Stockton (1978 and 1982) based on spectra with resolutions of 3 \AA for object A and $\sim 10 \text{ \AA}$ for the galaxies 1–3. Stockton did not quote uncertainties, but we estimate 1σ errors in those measurements of $\sim 0.5 \text{ \AA}$ (~ 0.0001 in the redshift) for object A and $\sim 1.5 \text{ \AA}$ (~ 0.0003 in the redshift) for the galaxies. The actual uncertainties for object A and galaxy 1 could be slightly larger because the line emission encompassing those sources is spatially blended and has a complex velocity structure (Hickson & Hutchings 1987; see also §3.3 below). Finally, we measured apparent AB magnitudes for all three of the brightest cluster galaxies in Figure 1 (numbers 1–3) to be $m_{AB} \approx 19.3 \pm 0.1$ at their rest-frame wavelength of $\sim 5000 \text{ \AA}$. These measurements imply absolute B-band magnitudes of $M_B \approx -19.3 \pm 0.1 + 5 \log(h)$ and luminosities of $L \approx 0.8 L_*$ (for $M_* = -19.5 + 5 \log[h]$) and no corrections for the spectral slopes; see Lonsdale & Chokshi 1993).

We obtained new *HST* and ground-based spectra of PKS 2135–147 with the goals of determining the location of the $z_a \approx z_e$ absorber and deriving its kinematics, ionization and metal abundances. We will show that the *HST* data provide significant new information compared to the *IUE* results, but the analysis is still hindered by modest spectral resolutions and the resulting uncertainties in the redshifts, absorption line profiles and column densities.

2. Observations and Results

2.1. UV Spectroscopy with *HST-FOS*

We observed PKS 2135–147 with the pre-COSTAR *HST*-Faint Object Spectrograph (FOS) on 1992 September 13. The spectra obtained through the $1''$ aperture use the high resolution gratings G130H² and G190H and provide complete wavelength coverage from 1140 to 2330 \AA at a resolution of $\lambda/\Delta\lambda \sim 1300$ (230 km s^{-1}). (The usable spectrum ends at $\sim 1220 \text{ \AA}$ where it is interrupted by strong geocoronal Ly α emission.) Figure 2 shows the combined *HST* spectrum (G130H + G190H) with the prominent $z_a \approx z_e$ absorption lines labeled. The total usable exposure times were 40 min with G130H and 36 min with G190H. The spectra were calibrated by the *Space Telescope Science Institute* using their standard “pipeline” procedures immediately after the observations. Those calibrations have wavelength uncertainties up to a few \AA . We corrected the wavelengths in the G130H spectrum by applying a uniform shift of -0.15 \AA , so that the Galactic absorption line Si II $\lambda 1260$ is at its laboratory wavelength in the measured spectrum. This shift is consistent with the centroid of the much broader (and less accurately measured) geocoronal Ly α line (1215.67 \AA). We corrected the G190H wavelengths by simultaneously requiring that (1) the one-component fits to the $z_a \approx z_e$ absorption lines in C IV have roughly the same redshift as N V in the wavelength-corrected G130H spectrum (§2.1.1 below), and (2) the narrow core of the He II $\lambda 1640$ emission line has a redshift consistent with He II $\lambda 4686$ and the other narrow emission lines in the Lick spectrum (§2.2.1 below). These requirements both indicate a wavelength shift of -0.50 \AA . All further discussions in this paper will involve the wavelength-corrected spectra.

2.1.1. Absorption Line Measurements

Figure 3 shows the spectral regions across Ly β -O VI, Ly α -N V and C IV on an expanded wavelength scale, together with polynomial fits to the local “continuum” (which include the broad emission lines) and gaussian fits to the $z_a \approx z_e$ absorption profiles³. Table

²The short-wavelength observation was originally scheduled for the Goddard High Resolution Spectrograph (GHRS) with the G140M grating, which would have provided higher resolution and greater sensitivity. However loss of operation of side 1 of GHRS necessitated the use of the FOS-G130H.

³All of the fits and measurements (here and in §2.2.1 below) were performed using the IRAF data analysis software (pro-

2 lists various line fitting results, including the centroid wavelengths (λ_{obs}), the absorption redshifts (z_a) based on the laboratory wavelengths in Verner *et al.* (1994), the rest equivalent widths (REW) and the full widths at half minimum (FWHM). We constrained the gaussian fits so that both members of the C IV, N V and O VI doublets have the same redshift and FWHM. The results from fitting each line with a single gaussian are given in the top half of Table 2. Ly α and C IV have weak secondary “notches” in their blue wings and are fit better with two gaussian components. Attempts at fitting the other $z_a \approx z_e$ lines with two components failed to yield unique results. The dotted curves in Figure 3 show the two-component fits to Ly α and C IV and one-component fits to the other lines. The results from the two-component fits are listed in the middle of Table 2. The bottom of the table provides data from a one-component fit to the Galactic absorption line Si II λ 1260, which is the only Galactic line detected in our spectra.

Lines searched for but not detected in the $z_a \approx z_e$ system at REW $< 0.3 \text{ \AA}$ (3σ) include Si II λ 1260, C II λ 1335 and Si IV $\lambda\lambda$ 1394,1403. Bergeron & Kunth (1983) reported small changes in the Ly α and C IV absorption lines between two *IUE* observations in 1979 and 1981. Our experience with similar *IUE* data suggests that those changes are not significant, especially if one allows for possible real changes in the underlying broad emission-line profiles. The *HST* measurements of the $z_a \approx z_e$ lines are the same as the overall *IUE* results within the uncertainties. We conclude that there is no convincing evidence for absorption-line variability.

2.2. Optical Spectroscopy at Lick Observatory

We obtained ground-based optical spectra of PKS 2135–147 on 1992 September 5 (8 days before the *HST* observations) at Lick Observatory using the Shane 3 m telescope and the KAST spectrograph. This spectrograph employs a dichroic beam-splitter to record the “blue” and “red” spectra simultaneously in two channels using 1200×400 pixel Reticon CCD detectors. We used a $2''$ entrance slit for our science ob-

vided by the National Optical Astronomy Observatories), including the supplemental program SPECFIT written by Gerald Kriss. Note that the use of gaussian profiles for fitting the unresolved or marginally resolved absorption lines is appropriate because the strong core of the FOS line spread function is well approximated by a gaussian (Evans 1993).

servations and a $6''$ slit for flux calibration (relative to standard stars). The data were reduced in the usual way using VISTA (Barlow 1993). Our highest resolution observations, used for measuring the emission-line redshifts below, cover $\sim 3240\text{--}4600 \text{ \AA}$ in the blue channel with a mean dispersion of 1.13 \AA per pixel and a resolution of FWHM $\sim 2.9 \text{ \AA}$. The corresponding red-channel spectrum spans $\sim 5130\text{--}6540 \text{ \AA}$ at 1.17 \AA per pixel and has resolution FWHM $\sim 3.0 \text{ \AA}$. These spectra are plotted in Figure 4. There is no evidence for Mg II $\lambda\lambda$ 2796,2803 absorption in the $z_a \approx z_e$ system above an upper limit of REW $\sim 0.4 \text{ \AA}$.

2.2.1. Emission Line Measurements

Table 3 lists the centroid wavelengths and redshifts of emission lines in the *HST* (He II λ 1640 only) and Lick spectra. The emission-line spectrum of PKS 2135–147 has a mixture of distinct broad and narrow line components; these are listed separately in the top and bottom portions of the table. We measured the line centroids using only the upper $\sim 80\%$ of the profiles (i.e. the line flux that lies above the continuum by more than $\sim 20\%$ of that line’s peak height). This procedure yields robust redshifts that are not sensitive to the uncertain continuum placement. [O III] λ 4959 and the narrow H β component both sit atop a broad H β emission profile. We measured the redshifts in these narrow lines by treating the broad H β emission as part of the continuum. We measured the broad H β itself by interpolating a curve through the base of the narrow H β component and using only the upper $\sim 50\%$ of the broad profile to avoid the portions that blend with [O III] in the red wing. The uncertainties in the wavelengths and redshifts listed in Table 3 reflect only the photon counting statistics. The 1σ uncertainties in the wavelength calibration are an additional $\sim 0.1 \text{ \AA}$.

The redshifts in Table 3 follow from the laboratory wavelengths in Verner *et al.* (1994), Osterbrock (1989), Wiese *et al.* (1966). We adopt a mean wavelength of 3727.4 \AA for the blended [O II] doublet, assuming the pair’s intrinsic flux ratio is unity. The mean redshift of the narrow emission lines in Table 3, excluding He II, is $z_e = 0.20032 \pm 0.00004$, which agrees well with the QSO redshifts of 0.20036 ± 0.00004 reported by Bergeron & Boisse (1986) and 0.2004 given by Stockton (1982).

We note in passing that the ratio of [O III] line fluxes, $(f(\lambda 4959) + f(\lambda 5007))/f(\lambda 4363)$, provides a temperature estimate for the narrow-line region in

PKS 2135–147. We measure $(f(\lambda 4959) + f(\lambda 5007)) / f(\lambda 4363) = 80 \pm 5$ from the spectrum in Figure 4, which corresponds to $T_e = 14,200 \pm 400$ K for densities $n_e \lesssim 10^5 \text{ cm}^{-3}$ (Osterbrock 1989). This result is consistent with the more plentiful observations of [O III] in Seyfert and radio galaxies (Tadhunter, Robinson & Morganti 1989, Storchi-Bergmann *et al.* 1996), and it supports the general finding that the [O III] temperatures are too high compared to simple photoionization models that assume low (less-than-critical) densities (e.g. Wilson 1996).

3. Discussion

3.1. Line Velocities and Redshifts

The best one-component fits to the $z_a \approx z_e$ lines have redshifts that are larger than the QSO’s forbidden-line redshift by about 150 km s^{-1} (compare Table 2 and 3). This difference is small compared to the absorption-line FWHMs, which range from roughly 350 to 550 km s^{-1} . A gaussian deconvolution of these FWHMs indicates line-of-sight velocity dispersions of 270 to 450 km s^{-1} . In the best two-components fits to Ly α and C IV, the individual absorption features are separated by $\sim 325 \text{ km s}^{-1}$ and straddle the QSO’s forbidden-line redshift. The redshift separation between these absorption components also encompasses the redshifts of companion A and the cluster galaxies 1–3 in Figure 1. The redshifts alone, therefore, fail to identify the absorber.

Nonetheless, the small velocity shift between the QSO and the $z_a \approx z_e$ gas could mean that the absorber is essentially at rest ($\pm 200 \text{ km s}^{-1}$) with respect to the QSO and therefore outside the deep gravitational potential of the QSO and its host-galaxy nucleus, at least a kpc away. However, absorption much nearer the QSO cannot be ruled out. The true space velocities might be much larger if they are dominated by rotation or infall/outflow that is mostly perpendicular to our line-of-sight to the QSO. For example, in the models of QSO outflows driven off of accretion disks (Shlosman *et al.* 1985, Murray *et al.* 1995), the gas velocities near the disk are dominated by rotation plus a small vertical component (perpendicular to the disk plane). Absorption lines measured along sightlines that graze the accretion disk might therefore have small line-of-sight velocities, even though the gas is participating in a high-velocity wind very near the QSO.

3.2. Projected Distances of the Cluster Galaxies

The projected distances of the cluster objects from PKS 2135–147 are $4.0h^{-1}$ kpc for object A and $12h^{-1}$, $36h^{-1}$ and $90h^{-1}$ kpc for galaxies 1, 2 and 3, respectively. Studies of low-redshift intervening ($z_a \ll z_e$) systems show that luminous ($\sim L_*$) galaxies like those near PKS 2135–147 can cause absorption lines with $\text{REW} \gtrsim 1.0 \text{ \AA}$ if they are close enough to our sightline to the QSO. In the survey by Lanzetta *et al.* (1995), 2 of 4 galaxies at projected distances $\lesssim 42h^{-1}$ kpc but none at larger distances produced strong ($\text{REW} \gtrsim 1.0 \text{ \AA}$) C IV absorption. Similarly, 5 of 5 galaxies at $\lesssim 80h^{-1}$ kpc and 7 of 9 at $\lesssim 100h^{-1}$ kpc gave rise to strong Ly α . For a situation like PKS 2135–147, where the QSO lies at the center of a cluster, we expect $\sim 50\%$ lower probabilities for the cluster galaxies producing $z_a \approx z_e$ lines because roughly half the galaxies will lie behind the QSO. Any given cluster galaxy has no more than a 50% chance of producing $z_a \approx z_e$ lines because of this ambiguity. The very limited statistics provided by Lanzetta *et al.* therefore suggest that galaxies 1 and 2 near PKS 2135–147 each have a $\sim 25\%$ chance of contributing significantly to the C IV absorption and a $\sim 50\%$ chance of contributing to Ly α . Similarly, the more distant galaxy 3 has a $\sim 25\%$ chance of contributing to Ly α but essentially no chance of causing strong C IV absorption.

These arguments based on projected distances suggest that the best candidate for the $z_a \approx z_e$ absorber is the diffuse halo surrounding object A and the QSO itself (Hickson & Hutchings 1987). However, the likelihood of such a halo producing $z_a \approx z_e$ lines is unknown. Presumably many (most?) QSOs have host-galaxy halos like PKS 2135–147, but only $\sim 25\%$ of radio-loud and even fewer radio-quiet QSOs have strong C IV absorption lines at $z_a \approx z_e$ (Foltz *et al.* 1988).

3.3. Line Optical Depths and Column Densities

The moderate resolution of the *HST*-FOS spectra ($\sim 230 \text{ km s}^{-1}$) necessarily leads to uncertainties in the measured profiles and derived column densities. The full widths of the $z_a \approx z_e$ lines appear marginally resolved in these data (Table 2), but narrow, unresolved line components could “hide” considerable column density while contributing little to the line equiv-

alent widths. In particular, line components with velocity widths as low as the thermal kinetic speeds of ~ 5 to ~ 20 km s $^{-1}$ could be present based on observations of intervening ($z_a \ll z_e$) metal-line systems (Blades 1988). The measured absorption line depths in PKS 2135–147, coupled with the N V and O VI doublet ratios and the Ly α /Ly β decrement, suggest that there are unresolved line components with large optical depths. The C IV doublet ratios are consistent with optically thin absorption, but that result is uncertain because the lines are blended and the shape of the underlying broad emission-line profile is unknown. The last two columns in Table 2 provide lower limits on the line-center optical depths (τ_0^{min}) and ionic column densities ($\log N^{min}$ in cm $^{-2}$) assuming that each line is fully resolved with the REW and FWHM given by our gaussian fits. These values of τ_0^{min} and $\log N^{min}$ follow from a simple curve-of-growth analysis, where the doppler b -values relate to the fitted FWHM by $b = \text{FWHM}/\sqrt{4 \ln 2}$. The column densities, although strictly just lower limits, are typical of high-redshift $z_a \approx z_e$ systems observed at much higher spectral resolutions from the ground (see Hamann 1997 and references therein).

3.4. Ionization

Bergeron & Boisse (1986) showed that the ionizing flux from the QSO in PKS 2135–147 overwhelms the intergalactic background radiation field throughout the cluster environment shown in Figure 1. They also showed that in this environment the QSO’s radiative flux can easily photoionize the gas up to C IV and N V if the densities are typical of galactic disks or halos and the distances from the QSO are comparable to the projected distances in Figure 1. Our *HST* measurement of strong O VI absorption indicates that even higher levels of ionization are present. The standard photoionization calculations plotted in Figure 2b of Hamann (1997) show that the ionization fractions of C IV, N V and O VI peak at ionization parameters of $U \approx 0.01$, 0.05 and 0.25, respectively (where U is defined as the dimensionless ratio of hydrogen-ionizing photon to hydrogen particle densities). Those calculations used an input spectrum believed to be typical of Seyfert nuclei and low-redshift QSOs (from Mathews & Ferland 1987). The harder incident spectrum used by Bergeron & Boisse (1986) in similar calculations leads to slightly higher ionization states at the same U , but the main results are the same. The strong presence of O VI requires gas densities that are 5 to

10 times smaller, or distances from the QSO that are 2 to 3 times shorter, than those needed for C IV and N V alone.

This level of ionization appears to be common in BALs and other $z_a \approx z_e$ systems that are known to be intrinsic (Weymann *et al.* 1985, Korista *et al.* 1996, Hamann 1997). However, it is also easily attained in the halos of the cluster galaxies near PKS 2135–147 via photoionization by the QSO. If we adopt a distance to PKS 2135–147 of $645h^{-1}$ Mpc and scale the Mathews & Ferland (1987) spectrum to match the observed fluxes in Figure 2, we find that the ionization parameter is related to the gas density, n_H , and the distance from the QSO, D , by, $U \approx 0.25h^{-2} \left(\frac{0.06 \text{cm}^{-3}}{n_H} \right) \left(\frac{20 \text{kpc}}{D} \right)^2$. The value of $U \approx 0.25$ needed for strong O VI is therefore within reach at low halo-like densities in the cluster galaxies. The most recent observations of intervening ($z_a \ll z_e$) metal-line absorbers show that ionizations up to O VI are commonplace even without the radiative flux of a nearby QSO (Lu & Savage 1993, Burles & Tytler 1996). Therefore the detection of strong O VI lines provides no insight into the location of the absorber.

The similar column densities derived for C IV, N V and O VI in Table 2 suggest that the absorber has a range of ionization states. A lower limit of $U \approx 0.003$ follows from the non-detections of C II and Mg II (see Fig. 2b in Hamann 1997). The larger derived column densities and stronger evidence for saturation in N V and O VI compared to C IV suggest that higher ionizations dominate. We can place an approximate upper limit on the ionization parameter by assuming (for the moment) that the absorber has a single ionization state. This upper limit follows from the minimum H I column density in Table 2 and the ($\sim 2\sigma$) upper limit on the total hydrogen column density $N_H \lesssim 10^{20}$ cm $^{-2}$ from soft X-ray observations (Rachen, Mannheim & Biermann 1996; for solar abundances). Together these results imply a neutral hydrogen fraction of H I/H $\gtrsim 3 \times 10^{-6}$, which corresponds to $U \lesssim 1$ (again, by Fig. 2b in Hamann 1997). Of course, a multi-phase absorber could still have components with little H I and much higher U . Future observations at shorter wavelengths could directly test for higher ionization components via the Ne VIII $\lambda\lambda 770,780$ doublet, which has been measured now in two other $z_a \approx z_e$ systems (Beaver *et al.* 1991, Hamann *et al.* 1995, Hamann *et al.* 1997c).

3.5. Metal Abundances

If we assume that at least the relative column densities in Table 2 are approximately correct, such that any saturation effects are the same for all lines, we can place lower limits on the metal abundances even with no knowledge of the ionization. Photoionization calculations (e.g. Hamann 1997, Bergeron & Stasińska 1986) show that the ionization corrections needed to convert the column density ratios (for example $N(\text{C IV})/N(\text{H I})$) into abundance ratios (C/H) always attain minimum values at some finite U . We can therefore derive the *minimum* metal abundances by adopting the *minimum* ionization corrections. Hamann (1997) calculated minimum correction factors for a wide range of incident QSO spectral shapes. Those calculations assume that the absorber is optically thin to continuum radiation at visible through far-UV wavelengths, which is consistent with the column densities in Table 2 and with the vast majority of well-measured $z_a \approx z_e$ systems at high redshift (Hamann 1997). (The column densities in Table 2 would have to be too low by $\gtrsim 2.5$ dex for H I [from Ly α] and by $\gtrsim 3.2$ dex for the metal ions to violate this assumption; cf. photoionization cross-sections in Osterbrock 1989.) The calculations are not sensitive to other (unknown) physical properties of the absorber. Applying the minimum correction factors from Figures 8 and 9 in Hamann (1997) to the column density ratio of $\log(N(\text{C IV})/N(\text{H I})) \approx 0.1$ from Table 2 implies a *minimum* abundance ratio of $[\text{C}/\text{H}] \approx 0.2 \pm 0.2$ (where $[\text{C}/\text{H}] = \log(\text{C}/\text{H}) - \log(\text{C}/\text{H})_\odot$). The $\sim 1\sigma$ uncertainty in this lower limit follows from the uncertainty in the QSO's flux distribution at important far-UV energies (see Hamann 1997 for discussion). The same analysis applied to N V and O VI leads to somewhat lower minimum values of $[\text{N}/\text{H}]$ and $[\text{O}/\text{H}]$ compared to the $[\text{C}/\text{H}]$ result. Keep in mind, however, that these results must be viewed with caution because of the uncertain column densities.

4. Summary and Conclusions

We use spectroscopic and imaging observations obtained with *HST* and at Lick Observatory to study the $z_a \approx z_e$ absorber in the $z_e \approx 0.20$ QSO PKS 2135–147. The *HST*-FOS spectra exhibit strong $z_a \approx z_e$ absorption lines of Ly α , Ly β , C IV $\lambda\lambda 1548, 1551$, N V $\lambda\lambda 1238, 1242$ and O VI $\lambda\lambda 1032, 1037$. There is no clear evidence for line variability between the *HST* and previous *IUE* observations. The full line widths are marginally

resolved in the *HST* spectrum, with deconvolved FWHM of 270 to 450 km s $^{-1}$. However, the N V and O VI doublet ratios, and the more uncertain Ly β /Ly α decrement, indicate that there are unresolved, optically thick line components. There is also direct evidence in the C IV and Ly α profiles for two blended absorption components. Lower limits on the total column densities (from a curve-of-growth analysis) range from $\log N(\text{H I}) \gtrsim 14.7 \text{ cm}^{-2}$ and $\log N(\text{C IV}) \gtrsim 14.8 \text{ cm}^{-2}$ to $\log N(\text{O VI}) \gtrsim 15.3 \text{ cm}^{-2}$. The C IV doublet ratio is consistent with no saturation, so the actual C IV column might be close to the lower limit.

Any analyses based on these column densities must be considered tentative because of the possible line saturation. Nonetheless, the similar derived columns in C IV, N V and O VI suggest that the absorber has a range of ionization states. If the gas is photoionized by the QSO, this range can be characterized by ionization parameters from $U \sim 0.01$ to at least 0.25. The upper limit is unknown, but a lower limit of $U \approx 0.003$ follows from the absence of C II and Mg II absorption. The larger minimum column density and stronger evidence for line saturation in O VI suggest that the higher ionization states dominate. The QSO could produce these ionization states by photoionization in environments ranging from near the central engine to the low-density halos of cluster galaxies tens of kpc away. Whatever the location or ionization state of the absorber, we show that the C/H abundance ratio must be at least solar if the gas is photoionized by the QSO and the derived *relative* column densities in H I and C IV are roughly accurate.

The source of the $z_a \approx z_e$ absorption remains uncertain. The redshifts spanned by the $z_a \approx z_e$ line profiles are consistent with contributions from the galactic halo surrounding the QSO and its compact companion, and/or from the halos of two $\sim L_*$ galaxies at projected distances $\leq 36h^{-1}$ kpc. The only firm conclusion from the redshift analysis is that the $z_a \approx z_e$ absorber has a line-of-sight velocity that is small (less than $\pm 200 \text{ km s}^{-1}$) with respect to the QSO. This small velocity shift could mean that the absorber lies outside the deep gravitational potential of the QSO and its host-galaxy nucleus, at least a kpc away. However, the $z_a \approx z_e$ absorber could be much closer to the QSO and the true space velocities could be much larger if the motions are mostly perpendicular to our line-of-sight (e.g. rotational). There is, in fact, indirect evidence favoring absorption near the QSO. In particular, PKS 2135–147

is a strong radio source with a steep radio spectrum and a lobe-dominated morphology (Morganti *et al.* 1993). These properties are known to correlate positively with both the strength and frequency of $z_a \approx z_e$ lines (Foltz *et al.* 1988, Wills *et al.* 1995, Barthel, Tytler & Vestergaard 1997), indicating that the absorbers in those cases are physically associated with the QSO and/or its host galaxy. The recent detections of time-variable $z_a \approx z_e$ lines in two radio-loud QSOs (Barthel *et al.* 1997, Aldcroft *et al.* 1997) suggest that the gas resides close to the QSO (Hamann *et al.* 1997a). In addition, the derived (tentative) metallicity in the PKS 2135–147 absorber is too high for an intervening galaxy halo (cf. Tytler 1988, Bergeron 1988) but typical of known or suspected intrinsic systems (Møller *et al.* 1994, Petitjean *et al.* 1994, Tripp *et al.* 1996, Turnshek *et al.* 1996, Korista *et al.* 1996, Hamann 1997). Furthermore, the strong N V absorption compared to C IV and O VI is common among known or suspected intrinsic absorbers (see Hamann 1997 and references therein) but extremely rare in intervening metal-line systems (excluding those with damped-Ly α ; Weymann *et al.* 1981, Hartquist & Snijders 1982, Sargent *et al.* 1988, Bergeron 1988, Bahcall *et al.* 1993, Lu & Savage 1993, Lanzetta *et al.* 1995, Burles & Tytler 1996).

Relatively strong N V lines are probably a good indicator of intrinsic versus intervening absorption in general. Weymann *et al.* (1981) and Hartquist & Snijders (1982) noted a strong observational trend for much larger N V/C IV line ratios in $z_a \approx z_e$ systems compared to $z_a \ll z_e$. This dichotomy cannot be understood simply in terms of higher ionization in $z_a \approx z_e$ absorbers because recent studies show that $z_a \ll z_e$ systems also typically have strong O VI lines and therefore considerable high-ionization gas (Lu & Savage 1993, Burles & Tytler 1996). N V is weak relative to both C IV and O VI in these systems. We propose that the lower N V/O VI and N V/C IV line ratios in intervening systems are caused by an underabundance of nitrogen (relative to solar ratios) in the low-metallicity galactic halos. Relatively higher nitrogen abundances and stronger N V absorption lines should occur naturally in the metal-rich environments of intrinsic absorbers, e.g. in the inner regions of the massive galaxies that host QSOs (Hamann & Ferland 1993, Vila-Costas & Edmunds 1993, Hamann 1997 and references therein). The combined N V/O VI and N V/C IV line ratios could, in fact, be used to

measure or constrain the N/O and N/C abundances. We must be cautious, however, because saturation effects in the intrinsic systems (§3.3) could mimic the proposed abundance differences by driving the intrinsic line ratios toward unity. Also, differences in the N V/O VI and N V/C IV line ratios between $z_a \approx z_e$ and $z_a \ll z_e$ systems might still derive from subtleties in the ionization rather than abundance effects. For example, in galaxy halos that are not near QSOs, N V might fall in a narrow ionization “gap” between a photoionized gas component that produces mainly C IV and the lower ions and a hot, collisionally ionized component that produces O VI (Burles & Tytler 1996). N V might then be stronger in halos near QSOs because of the increased *photo*-ionization. Such halo-near-QSO systems would not meet our definition of intrinsic, and would not be expected to have enhanced nitrogen abundances, even though their N V lines are strong.

Further observations are needed to clearly identify the $z_a \approx z_e$ absorber in PKS 2135–147. For example, higher resolution spectra of the QSO and the cluster galaxies would allow us to (1) measure and compare the redshifts more precisely, (2) determine whether the $z_a \approx z_e$ lines have narrow, multi-component profiles typical of intervening metal-line systems (Blades 1988) or smooth and relatively broad profiles like some known intrinsic systems (Hamann *et al.* 1997a, 1997b and 1997c), (3) carefully examine the multiplet ratios to test for partial line-of-sight coverage of the background light source as another indicator of intrinsic absorption (Hamann *et al.* 1997a, Hamann *et al.* 1997b, Barthel *et al.* 1997), and (4) derive accurate column densities for the abundance and ionization analyses. Monitoring the QSO for line strength changes, particularly in response to continuum changes, might not only confirm the intrinsic hypothesis but place quantitative constraints on the absorber’s density, ionization and distance from the QSO (Barlow *et al.* 1992, Hamann *et al.* 1995, Hamann *et al.* 1997a, Hamann *et al.* 1997b).

We are grateful to the referee, T. Aldcroft, for suggestions that improved this manuscript. The *HST* spectra presented here were obtained through the Goddard High Resolution Spectrograph Guaranteed Time program. This research was supported by NASA grants NAG 5-1630, NAG 5-1858 and NAG 5-3234.

TABLE 1
COORDINATES IN THE PKS 2135–147 FIELD

Source ^a	— Epoch 2000 —		Comment ^b
	R.A.	Dec.	
PKS ^c	21 37 45.248	−14 32 55.70	QSO ($z_e = 0.2003$)
A	21 37 45.353	−14 32 56.80	affected by QSO flux, ($z_e = 0.2003$)
1	21 37 45.585	−14 32 58.35	($z_e = 0.1997$)
2	21 37 44.732	−14 32 40.31	($z_e = 0.2002$)
3	21 37 47.238	−14 33 26.71	multiple flux peaks, ($z_e = 0.2008$)
4	21 37 42.969	−14 32 38.99	core not well defined
5	21 37 43.366	−14 32 29.76	
6	21 37 43.599	−14 33 01.69	
7	21 37 44.328	−14 32 49.75	
8	21 37 44.340	−14 33 18.64	
9	21 37 45.223	−14 32 38.27	point source
10	21 37 45.277	−14 32 34.68	faint
11	21 37 45.935	−14 32 32.75	
12	21 37 46.167	−14 33 17.40	
13	21 37 46.483	−14 33 05.67	point source
14	21 37 46.511	−14 32 42.39	blended with #15
15	21 37 46.516	−14 32 42.02	brighter of pair
16	21 37 46.563	−14 33 28.98	
17	21 37 47.018	−14 33 13.85	
18	21 37 47.165	−14 32 42.32	point source
19	21 37 48.053	−14 32 42.37	point source

^aGalaxy designations 1–3 follow Stockton (1978).

^bOnly obvious point sources (with diffraction spikes) are noted as such.

^cThe coordinates of the radio core are RA: 21 37 45.1, Dec: −14 32 55.6 (Morganti *et al.* 1993).

TABLE 2
ABSORPTION LINE RESULTS

Line	λ_{obs} (Å)	z_a	REW (Å)	FWHM (km s ⁻¹)	τ_0^{min}	$\log N^{min}$ (cm ⁻²)
One-Component Fits						
Ly β 1025.72	1231.37 \pm 0.16	0.20049 \pm 0.00016	1.83 \pm 0.28	709 \pm 146	1.0	15.5
O VI 1031.93	1239.08 \pm 0.08	0.20074 \pm 0.00008	1.14 \pm 0.14	432 \pm 56	1.0	15.1
O VI 1037.62	1245.91 \pm 0.08	...	1.17 \pm 0.14	...	1.0	15.4
Ly α 1215.67	1459.64 \pm 0.04	0.20069 \pm 0.00003	1.71 \pm 0.06	510 \pm 21	1.1	14.7
N V 1238.82	1487.73 \pm 0.05	0.20093 \pm 0.00004	1.06 \pm 0.08	351 \pm 32	0.9	14.8
N V 1242.80	1492.51 \pm 0.05	...	1.01 \pm 0.09	...	0.9	15.1
C IV 1548.20	1859.33 \pm 0.06	0.20092 \pm 0.00004	2.01 \pm 0.07	549 \pm 27	0.9	14.8
C IV 1550.88	1862.42 \pm 0.08	...	1.01 \pm 0.06	...	0.4	14.8
Two-Component Fits						
Ly α 1215.67	1458.28 \pm 0.10	0.19957 \pm 0.00008	0.37 \pm 0.10	229 \pm 55	0.4	13.9
Ly α 1215.67	1459.83 \pm 0.05	0.20084 \pm 0.00004	1.32 \pm 0.09	381 \pm 28	1.2	14.5
C IV 1548.20	1857.43 \pm 0.18	0.19974 \pm 0.00012	0.57 \pm 0.15	307 \pm 83	0.4	14.2
C IV 1550.88	1860.51 \pm 0.18	...	0.39 \pm 0.16	...	0.3	14.3
C IV 1548.20	1859.50 \pm 0.08	0.20108 \pm 0.00005	1.27 \pm 0.14	330 \pm 30	1.0	14.6
C IV 1550.88	1862.59 \pm 0.08	...	0.81 \pm 0.09	...	0.5	14.7
Galactic Lines						
Si II 1260.42	1260.42 \pm 0.11	0.00000 \pm 0.00008	0.69 \pm 0.16	224 \pm 58	0.9	13.7

TABLE 3
EMISSION LINE REDSHIFTS

Line	λ_{obs}	z_e
Narrow Lines		
He II 1640.4	1969.2 ± 0.3	0.2004 ± 0.0002
[Ne V] 3425.9	4112.0 ± 0.3	0.2003 ± 0.0001
[O II] 3727.4	4474.1 ± 0.3	0.2003 ± 0.0001
He II 4685.7	5624.3 ± 0.5	0.2003 ± 0.0001
H β 4861.3	5835.0 ± 0.6	0.2003 ± 0.0001
[O III] 4958.9	5952.4 ± 0.1	0.2003 ± 0.0001
[O III] 5006.9	6010.0 ± 0.1	0.2003 ± 0.0001
Broad Lines		
Mg II 2799.2	3363.1 ± 0.7	0.2014 ± 0.0002
H β 4861.3	5844.2 ± 1.2	0.2022 ± 0.0002

REFERENCES

- Aldcroft, T., Bechtold, J., & Foltz, C. 1997, in *Mass Ejection From AGN*, eds. R. Weymann, I. Shlosman, and N. Arav, ASP Conf. Series, in press
- Anderson, S. F., Weymann, R. J., Foltz, C. B., & Chaffee Jr., F. H. 1987, *AJ*, 94, 278
- Bahcall, J. N., *et al.* 1993, *ApJS*, 87, 1
- Bahcall, J. N., Kirhakos, S., & Schneider, D. P. 1997, in preparation
- Barlow, T. A. 1993, *Ph.D. Dissertation*, University of California – San Diego, p. 57
- Barlow, T. A., Junkkarinen, V. T., Burbidge, E. M., Weymann, R. J., Morris, S. L., & Korista, K. T. 1992, *ApJ*, 397, 81
- Barlow, T. A., & Sargent, W. L. W. 1997, *AJ*, 113, 136
- Barthel, P. D., Tytler, D. R., & Vestergaard, M. 1997, in *Mass Ejection From AGN*, eds. R. Weymann, I. Shlosman, and N. Arav, ASP Conf. Series, in press
- Beaver, E. A., *et al.* 1991, *ApJ*, 377, L1
- Bergeron, J. 1988, in *QSO Absorption Lines: Probing the Universe*, eds. J.C. Blades, C. Norman, & D.A. Turnshek, (Cambridge: Cambridge Univ. Press), 127
- Bergeron, J., & Boisse, P. 1986, *A&A*, 168, 6
- Bergeron, J., & Kunth, D. 1983, *MNRAS*, 205, 1053
- Bergeron, J. & Stasińska, G. 1986, *A&A*, 169, 1
- Blades, J. C. 1988, in *QSO Absorption Lines: Probing the Universe*, eds. J.C. Blades, C. Norman, & D.A. Turnshek, (Cambridge: Cambridge Univ. Press), 147
- Burles, S. & Tytler, D. 1996, *ApJ*, 460, 584
- Dunlop, J. S., Taylor, G. L., Hughes, D. H., & Robson, E. I. 1993, *MNRAS*, 264, 455
- Evans, I. N. 1993, *FOS Instrument Science Rep.*, CAL/FOS-104.
- Ferland, G. J., Baldwin, J. A., Korista, K. T., Hamann, F., Carswell, R. F., Phillips, M., Wilkes, B., & Williams, R. E. 1996, *ApJ*, 461, 683
- Fisher, K. B., Bahcall, J. N., Kirhakos, S., & Schneider, D. P. 1996, *ApJ*, 468, 469
- Foltz, C. B., Chaffee Jr., Weymann, R. J., & Anderson, S. F. 1988, in *QSO Absorption Lines: Probing the Universe*, eds. J. C. Blades, D. A. Turnshek, & C. A. Norman (Cambridge: Cambridge Univ. Press), 53
- Foltz, C. B., Weymann, R. J., Peterson, B. M., Sun, L., Malkan, M. A., & Chaffee, F. H., Jr. 1986, *ApJ*, 307, 504
- Hamann, F. 1997, *ApJS*, 109, 279
- Hamann, F., Barlow, T. A., Beaver, E. A., Burbidge, E. M., Cohen, R. D., Junkkarinen, V., & Lyons, R. 1995, *ApJ*, 443, 606
- Hamann, F., Barlow, T. A., Junkkarinen, V. T., & Burbidge, E. M. 1997a, *ApJ*, 478, 80
- Hamann, F., Barlow, T. A., & Junkkarinen, V. T. 1997b, *ApJ*, 478, 87
- Hamann, F., Barlow, T. A., Cohen, R. D., Junkkarinen, V. T., & Burbidge, E. M. 1997c, in *Mass Ejection From AGN*, eds. R. Weymann, I. Shlosman, and N. Arav, ASP Conf. Series, in press
- Hamann, F., & Ferland, G. J. 1993, *ApJ*, 418, 11
- Hartquist, T. W., & Sniijders, M. A. J. 1982, *Nature*, 299, 783
- Hickson, P. & Hutchings, J. B. 1987, *ApJ*, 312, 518
- Hutchings, J. B., & Neff, S. G. 1992, *AJ*, 104, 1
- Korista, K. T., Hamann, F., Ferguson, J., & Ferland, G. J. 1996, *ApJ*, 461, 641
- Lanzetta, K. M., Bowen, D. V., Tytler, D., and Webb, J. K. 1995, *ApJ*, 442, 538
- Lonsdale, C. J., & Chokshi, A. 1993, *AJ*, 105, 1333
- Lu, L., & Savage, B. D. 1993, *ApJ*, 403, 127
- Mathews, W. G., & Ferland, G. J. 1987, *ApJ*, 323, 456
- Møller, P., Jakobsen, P., & Perryman, M. A. C., 1994, *A&A*, 287, 719
- Morganti, R., Killee, N. E. B., & Tadhunter, C. N. 1993, *MNRAS*, 263, 1023

- Murray, N., Chiang, J., Grossman, S. A., & Voit, G. M. 1995, *ApJ*, 451, 498
- Morris, S. L., Weymann, R. J., Foltz, C. B., Turnshek, D. A., Shectman, S., Price, C., & Boroson, T. A. 1986, *ApJ*, 310, 40
- Osterbrock, D. E. 1989, *Astrophysics of Gaseous Nebulae and Active Galactic Nuclei*, (Mill Valley, CA: Univ. Sci. Press)
- Petitjean, P., Rauch, M., & Carswell, R. F. 1994, *A&A*, 291, 29
- Rachen, J. P., Mannheim, K., & Biermann, P. L. 1996, *A&A*, 310, 371
- Sargent, W. L. W., Boksenberg, A., & Steidel, C. C. 1988, *ApJS*, 68, 539
- Shlosman, I., Vitello, P. A., & Shaviv, G. 1985, 294, 96
- Smith, E. P., & Heckman, T. M. 1990, *ApJ*, 348, 38
- Stockton, A. 1978, *ApJ*, 223, 747
- Stockton, A. 1982, *ApJ*, 275, 33
- Stockton, A., & MacKenty, J. W. 1987, *ApJ*, 316, 584
- Storchi-Bergmann, T., Wilson, A. S., Mulchaey, J. S., & Binette, L. 1996, *A&A*, 312, 357
- Tadhunter, C. N., Robinson, A., & Morganti, R. 1989, in *Extranuclear Activity in Galaxies*, ESO Conf. and Workshop Proc. 32, eds. E. J. A. Meurs & R. A. E. Fosbury, 293 (Garching bei München, European Southern Obs.)
- Tripp, T. M., Lu, L., & Savage, B. D. 1996, *ApJS*, 102, 239
- Turnshek, D. A. 1988, in *QSO Absorption Lines: Probing the Universe*, eds. J. C. Blades, D. A. Turnshek, & C. A. Norman (Cambridge: Cambridge Univ. Press), 17
- Turnshek, D. A., Kopko, M., Monier, E., Noll, D., Espey, B., & Weymann, R. J. 1996, *ApJ*, 463, 110
- Tytler, D. 1988, in *QSO Absorption Lines: Probing the Universe*, eds. J.C. Blades, C. Norman, & D.A. Turnshek, (Cambridge: Cambridge Univ. Press), 179
- Verner, D., Barthel, P. D., & Tytler, D. 1994, *A&AS*, 108, 287
- Véron-Cetty, M.-P., & Woltjer, L. 1990, *A&A*, 236, 69
- Vila-Costas, M. B., & Edmunds, M. G. 1993, *MNRAS*, 265, 199
- Weymann, R. J., Carswell, R. F., & Smith, M. G. A. 1981, *ARA&A*, 19, 41
- Weymann, R. J., Morris, S. L., Foltz, C. B., & Hewett, P. C. 1991, *ApJ*, 373, 23
- Weymann, R. J., Turnshek, D. A., & Christiansen, W. A. 1985, in *Astrophysics of Active Galaxies and Quasi-Stellar Objects*, ed. J. Miller, (Mill Valley, CA: University Science Books), 185
- Weymann, R. J., Williams, R. E., Peterson, B. M., & Turnshek, D. A. 1979, *ApJ*, 218, 619
- Wiese, W. L., Smith, M. W., & Glennon, B. M. 1966, *Atomic Transition Probabilities (NBS-NSRDS 4, vol. 1)* (Washington: GPO)
- Williams, R. E., Strittmatter, P. A., Carswell, R. F., & Craine, E. R. 1975, *ApJ*, 202, 296
- Wills, B. J., *et al.* 1995, *ApJ*, 447, 139
- Wilson, A. S. 1996, in *Emission Lines in Active Galaxies: New Methods and Techniques*, IAU Colloq. 159, eds. B. M. Peterson, F.-Z. Cheng, and A. S. Wilson, ASP Conf. Series, 113, 264

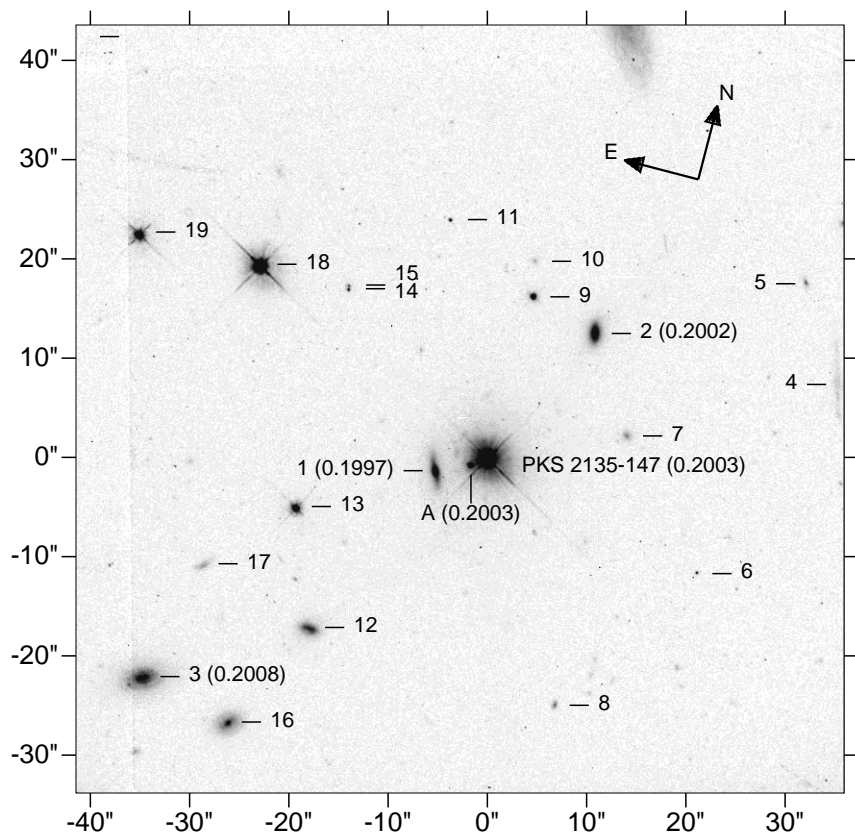
Figure Captions

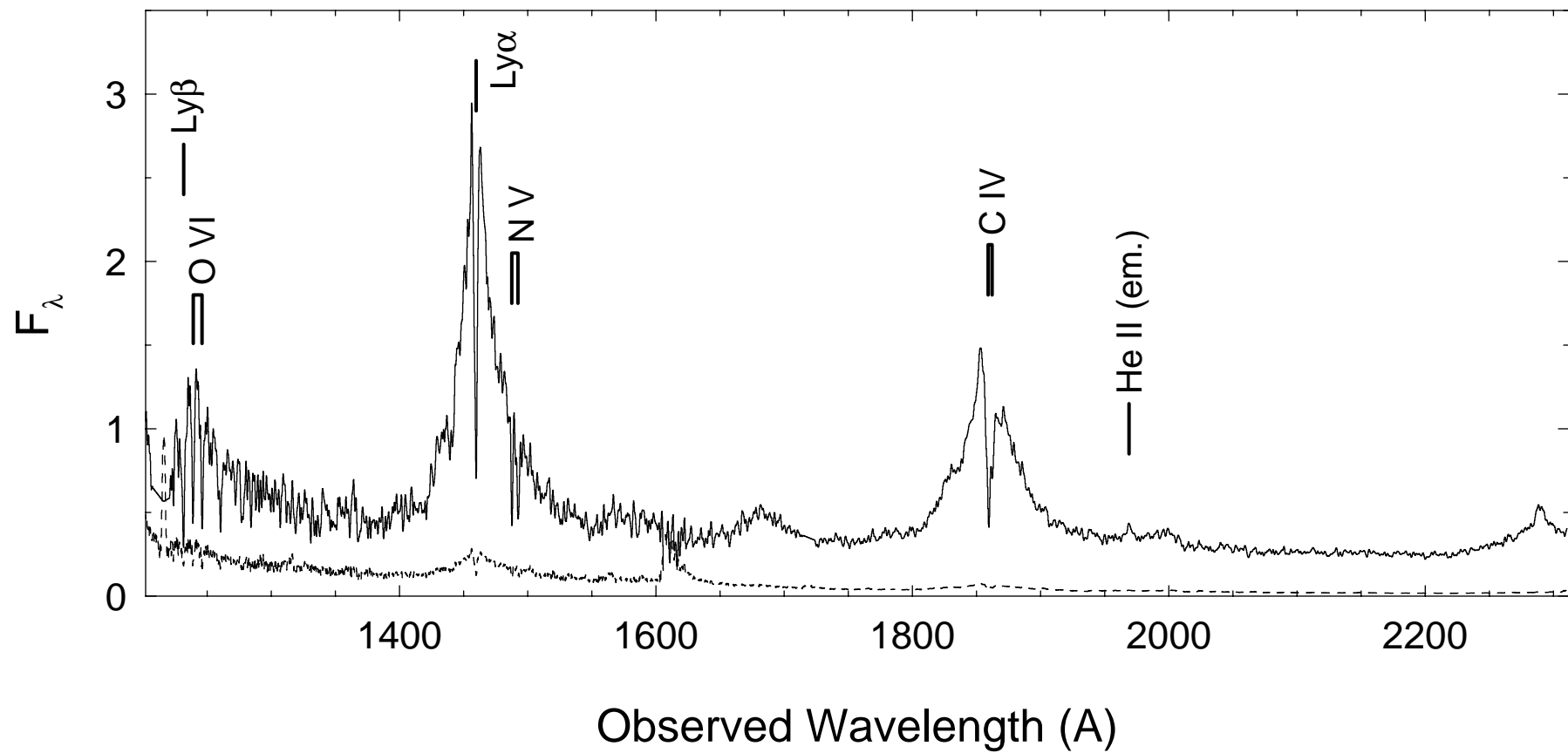
Fig. 1.— PKS 2135–147 field measured with *HST*-WFPC2 and a broad-band filter (F606W) centered at roughly 6060 Å. The vertical “stretch” is linear. The angular scale is in arcsec relative to the QSO position. (The linear scale at the QSO redshift is $\sim 2.2h^{-1}$ kpc arcsec $^{-1}$.) Redshifts are shown in parenthesis for the QSO (this paper), the compact object A (from Stockton 1982) and the galaxies 1–3 (Stockton 1978). The coordinates of all labeled sources are listed in Table 1. Separate CCD images join along the vertical line at $-36''$ and along a horizontal line at $+39''$.

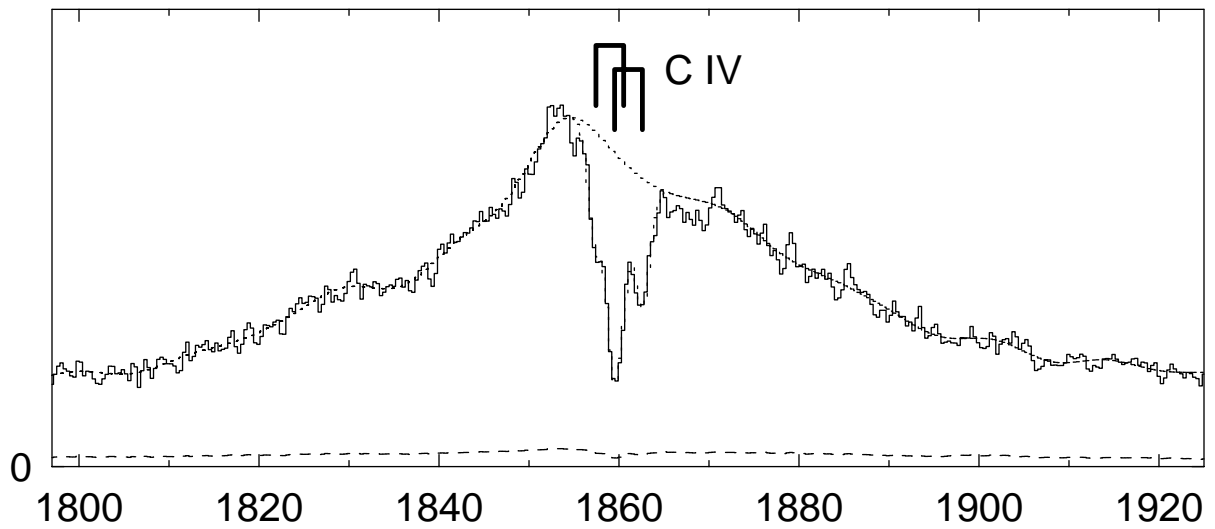
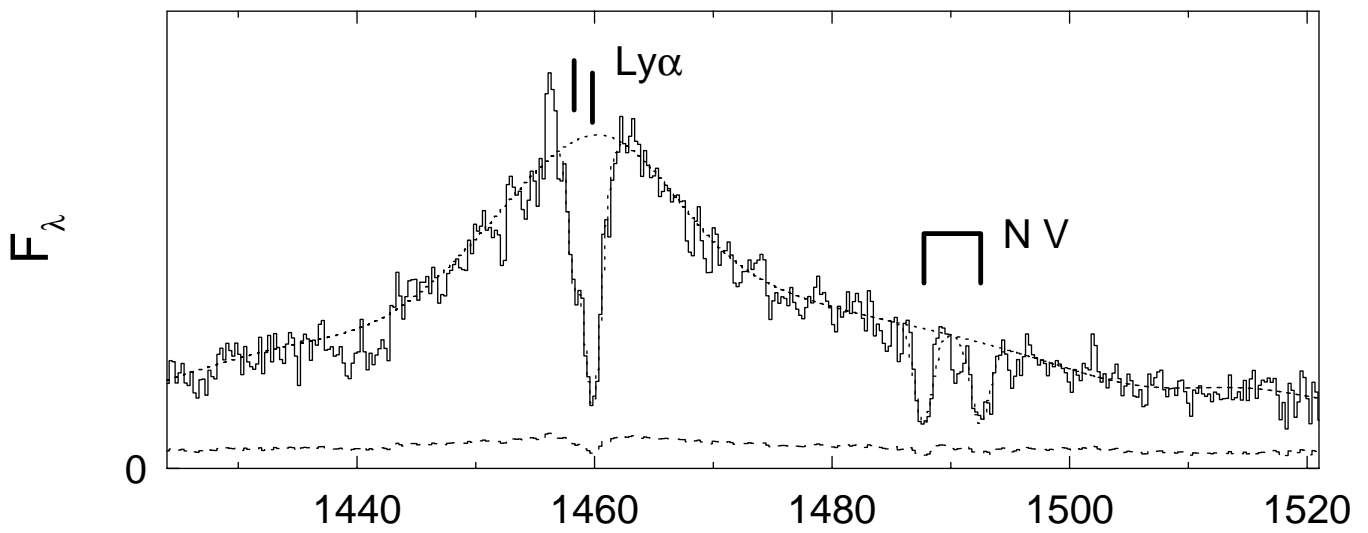
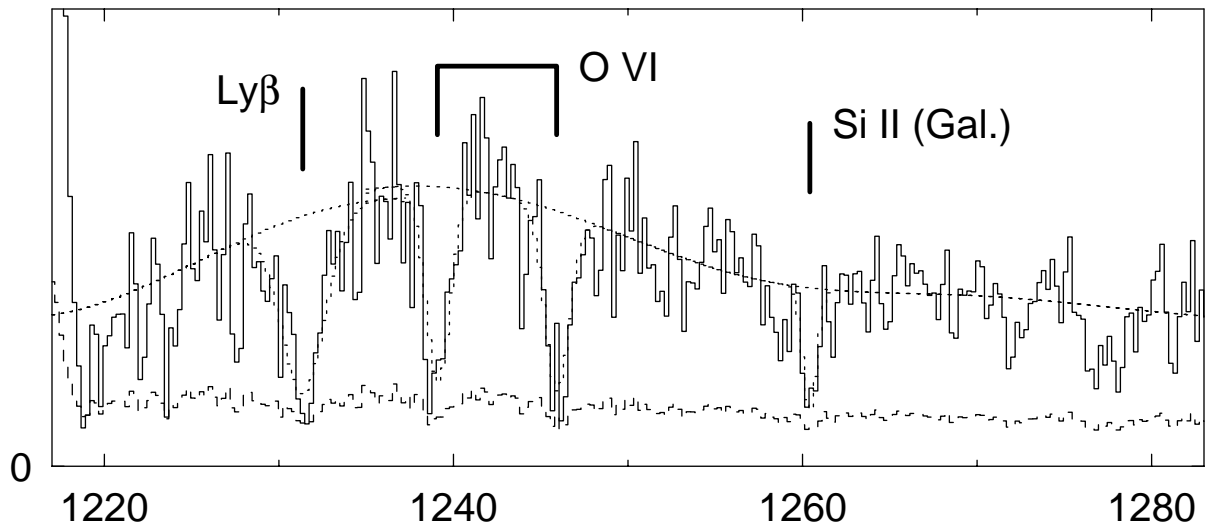
Fig. 2.— Combined *HST*-FOS spectrum of PKS 2135–147 obtained with the G130H and G190H gratings of the FOS. The associated absorption lines and the narrow He II emission line are labeled above. The spectra are shown after smoothing twice (G190H) and 3 times (G130H) with a 3-pixel wide boxcar function. The 1σ error spectrum (not smoothed) is shown by the dashed curve at the bottom. The associated absorption lines and the narrow He II emission line are labeled above. F_λ has units 10^{-14} ergs s $^{-1}$ cm $^{-2}$ Å $^{-1}$. The segment between roughly 1710 and 1725 Å is a straight-line interpolation across a detector noise spike.

Fig. 3.— *HST*-FOS spectra of PKS 2135–147 centered near the Ly β -O VI (top panel), Ly α -N V (middle panel) and C IV (bottom panel) absorption lines. The dashed curve at the bottom of each panel is the 1σ error spectrum. The dotted curves show the fits to the continuum and the absorption lines discussed in the text. The lines are labeled at the redshifts derived from the gaussian fits, with two components for Ly α and C IV. The panel also shows the Galactic Si II 1260.42 Å line used to set the wavelength scale.

Fig. 4.— Red and blue channel Lick spectra of PKS 2135–147. The flux units are 10^{-15} ergs s $^{-1}$ cm $^{-2}$ Hz $^{-1}$. The flux scale at the right corresponds to the upper spectrum in the bottom panel. The dashed curve at the bottom of each panel is the 1σ error spectrum. The emission lines are labeled at $z_e = 0.2003$.







Observed Wavelength (Å)

